2ar

UCID-16377

LAWRENCE LIVERMORE LABORATORY
University of California/Livermore, California

HIGH-PRESSURE MECHANICAL PROPERTIES OF AN AREA 12, NEVADA TEST SITE TUFF

A. Duba
A. E. Abey
H. C. Heard

November 19, 1973

Prepared for U. S. Atomic Energy Commission under contract no. W-7405-Eng-48

DISCLAIMER

HIGH PRESSURE MECHANICAL PROPERTIES OF AN AREA 12, NEVADA TEST SITE TUFF

ABSTRACT

The mechanical properties of tuff from instrument hole UG3, tunnel U12e.06 at the Nevada Test Site have been investigated to 1400 MPa. The shear strength increases from about 5 MPa unconfined to 12 MPa at 300 MPa mean pressure. A brittle-ductile transition was indicated at about 280 MPa. In uniaxial strain, the sample loads to the vicinity of the failure envelope and then is parallel to that envelope up to the highest stresses, 420 MPa. Hydrostatic pressure of 1400 MPa produces about 9% volume compression and 1.3% permanent compaction in this apparently saturated tuff.

INTRODUCTION

Major concerns in the underground nuclear testing program of the Defense Nuclear Agency (DNA) are stemming and containment. To adequately model ground motions relevant to these problems, the high pressure mechanical properties of the surrounding media are needed as input to numerical code calculations. Here, we describe the behavior of tuff from tunnel U12e.06, instrument hole UG3, Area 12, Nevada Test Site. The following tests were performed at strain rates of about 10^{-4}/s: (1) the pressure-volume (P-V) relationship on loading to and unloading from 100 and 1400 MPa, (2) the failure envelope to 300 MPa, (3) uniaxial stress loading paths at 0.1, 20, 30, 50, and 100 MPa to near failure with subsequent unloading, and (4) uniaxial strain loading and unloading paths to and from 80 and 420 MPa confining pressure.

The tuff was received as NX cores (~ 50-mm diam) wrapped in foil and coated with beeswax. Apparent water saturation of the cores was determined as 100% by measuring and weighing portions of each core as received, after drying at 85°C for 20 h, and after resaturation with water at a pressure of about 0.1 MPa. Samples were cut and cored using water as coolant, and the saturation was maintained by storing over water in a sealed container. The average density of the samples prepared from these cores (cores used in these tests were from depths of 14.2 to 14.7 m and 17.5 to 17.9 m) was 1.87 ± 0.03 Mg/m^3. The dry density was 1.54 ± 0.04 Mg/m^3, indicating about 18% water by weight or 33% by volume.

EXPERIMENTAL PROCEDURE

The samples used in all tests were fabricated into right circular cylinders 20 to 30 mm in diam and 30 to 100 mm long. For the uniaxial stress, uniaxial strain, and P-V measurements, 0.5-mm-thick lead jackets were fitted to the rock by application of a pressure of 0.4 MPa. The failure envelope was determined from samples jacketed with tygon. In each case, the jacket strength was considered in the data reduction process. The P-V relationship to hydrostatic pressures of 1400 MPa was determined from measurements made by foil strain gages bonded to jacketed specimens. Uniaxial strain loading and uniaxial stress loading were performed on similarly jacketed and instrumented samples. Hydrostatic pressure, either constant or increasing (depending on the type of test), was maintained while uniaxial loading was accomplished with a solid piston. The locus of failure points based on the principal stresses from uniaxial stress tests was used to determine the shear strength-mean pressure failure envelope. Experimental procedures and techniques are discussed in detail elsewhere.[1-5]

PRESSURE-VOLUME CHARACTERISTICS

The P-V relationship for the tuff from both the 14.2- to 14.7-m and 17.5- to 17.9-m levels was measured as a function of hydrostatic loading and unloading to pressures of either 100 or 1400 MPa. In some samples loaded to 100 MPa, extremely unusual unloading paths were noted. The sample either unloaded to a higher volume than its starting point, yielding an apparent negative permanent compaction; or the unloading curve criss-crossed the loading curve. This tuff is very heterogeneous and some samples contain large pumice fragments. If the pumice fragments have a relatively large air-filled porosity, they would undergo more compression on loading than the water which saturates the non-air-filled pores. The compression of the pumice results in pore collapse, producing permanent compaction of the pumice. However, upon unloading, the expansion of the collapsed pumice is less than that of water; thus, an originally "saturated" rock becomes supersaturated. We believe that the unusual unloading paths observed in this study result from excess water decoupling the jacket from some of the samples upon unloading. Eight of the 13 samples loaded to 100 MPa showed what is considered "normal" unloading behavior (Fig. 1). After unloading from 100 MPa, all samples showed less than 1% permanent volume change, whether compaction or expansion.

Figure 1 shows the P-V relationship for this tuff to 100 MPa. The rather large error bar for the unloading portion is the consequence of the unusual unloading behavior. Figure 2 shows the P-V relationship to 1400 MPa. No unusual unloading behavior was observed in samples loaded to this pressure. The magnitude of the water transition at about 1100 MPa indicates a free water content of about 10% by volume, which is less than one-third the total water indicated by the density determinations. Between

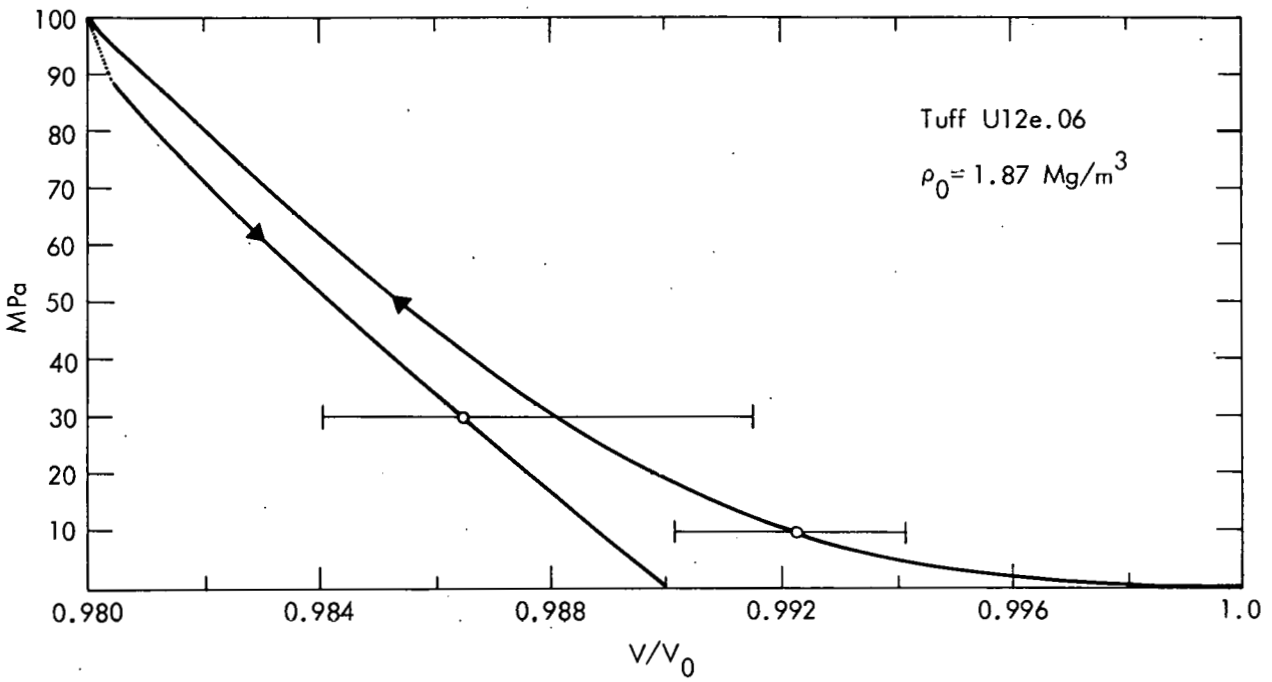

Fig. 1. Pressure (to 100 MPa) vs V/V_0 for U12e.06 tuff. Plot based on data from 13 samples.

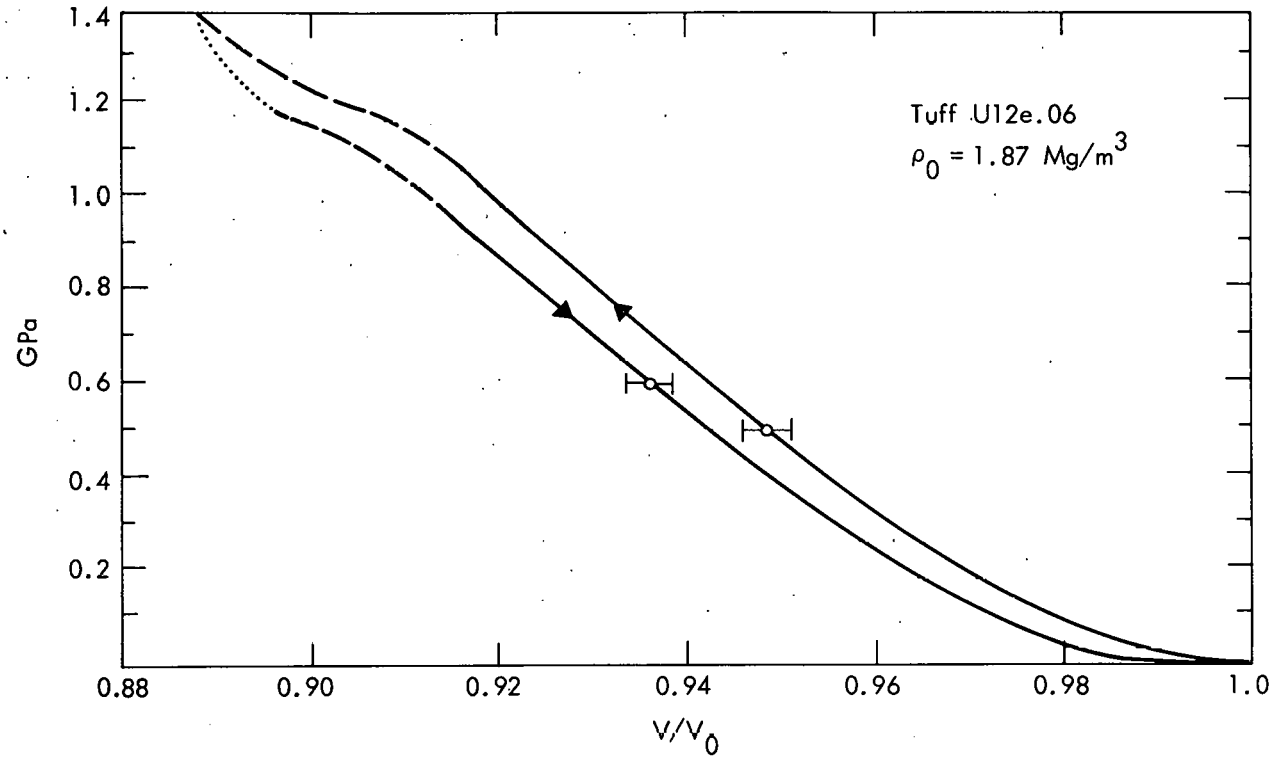

Fig. 2. Pressure (to 1400 MPa) vs V/V_0 for U12e.06 tuff, based on one test. Because of the water-ice transition (indicated by dashed lines) it was not possible to collect continuous data on unloading from 1400 to 1200 MPa (dotted line).

Table 1. Bulk modulus K as a function of pressure for tuff U12e.06.

Pressure (MPa)	K (GPa)
0.1	0.65
5	2.3
10	3.7
30	6.7
60	8.7
100	10.0
200	12.3
500	15.5
1000	18.7

0.1 and 1050 MPa, the P-V curve indicates a monotonically increasing bulk modulus K. The value of K, initially 0.65 GPa, increases to 19 GPa at 1000 MPa confining pressure. Table 1 lists K at several pressures as determined graphically from Fig. 2.

UNIAXIAL STRESS MEASUREMENTS (FAILURE)

Two types of tests were made to determine the failure behavior of samples of the core from 14.2 to 14.7 m. The first involved uniaxial compression of tygon-jacketed samples at confining pressures up to 300 MPa. The second type was the indirect tensile (Brazil) test. Although the latter test was performed only at atmospheric pressure (0.1 MPa), the calculated tensile strengths are believed to be relatively independent of confining pressure σ_2.[6]

Values for the maximum principal stresses at the failure point for each test type define the shear stress-mean pressure failure ($\tau - P_m$) envelope shown in Fig. 3. Although it has been demonstrated that the shear stress determined at failure for several different rock types is influenced by the relative value of σ_2 compared to σ_1 and σ_3,[6,7] the effect of σ_2 becomes important only at pressures much greater than 0.1 MPa. Thus, the Brazil test at atmospheric pressure may be safely included with the compression results.

The dominant failure mechanism for all tests at pressures less than 200 MPa was by a combination of shear and tensile fractures resulting in loss of cohesion of the sample. At the highest pressure attempted (300 MPa) no through-going fractures were noted after the test, although at least 10% axial strain was attained. We observed that this sample was barrelled and possessed excellent cohesion. Because the sample at 200 MPa was intermediate to the two extremes just discussed, the transition from brittle to ductile behavior is judged to occur at pressures somewhat greater than 200 MPa but less than 300 MPa (Fig. 3). Ductile behavior is defined as 5% axial strain beyond the elastic limit.[8] The failure data are summarized in Table 2.

The shear strength-mean pressure failure envelope for the saturated U12e.06 tuff is 10 to 40 MPa at 300 MPa mean pressure (Fig. 3), which is lower than that reported for Area 16, NTS tuffs.[9,10] Although of similar grain size and appearance as the U12e.06 tuff, the Area 16 tuffs were only about 85% saturated. We believe the marked difference in shear strength among all these tuffs to be a consequence primarily of water saturation. Fine-grained Mt. Helen tuff shows an inverse correlation of shear strength with water content[11] and has a shear strength (saturated) ranging up to

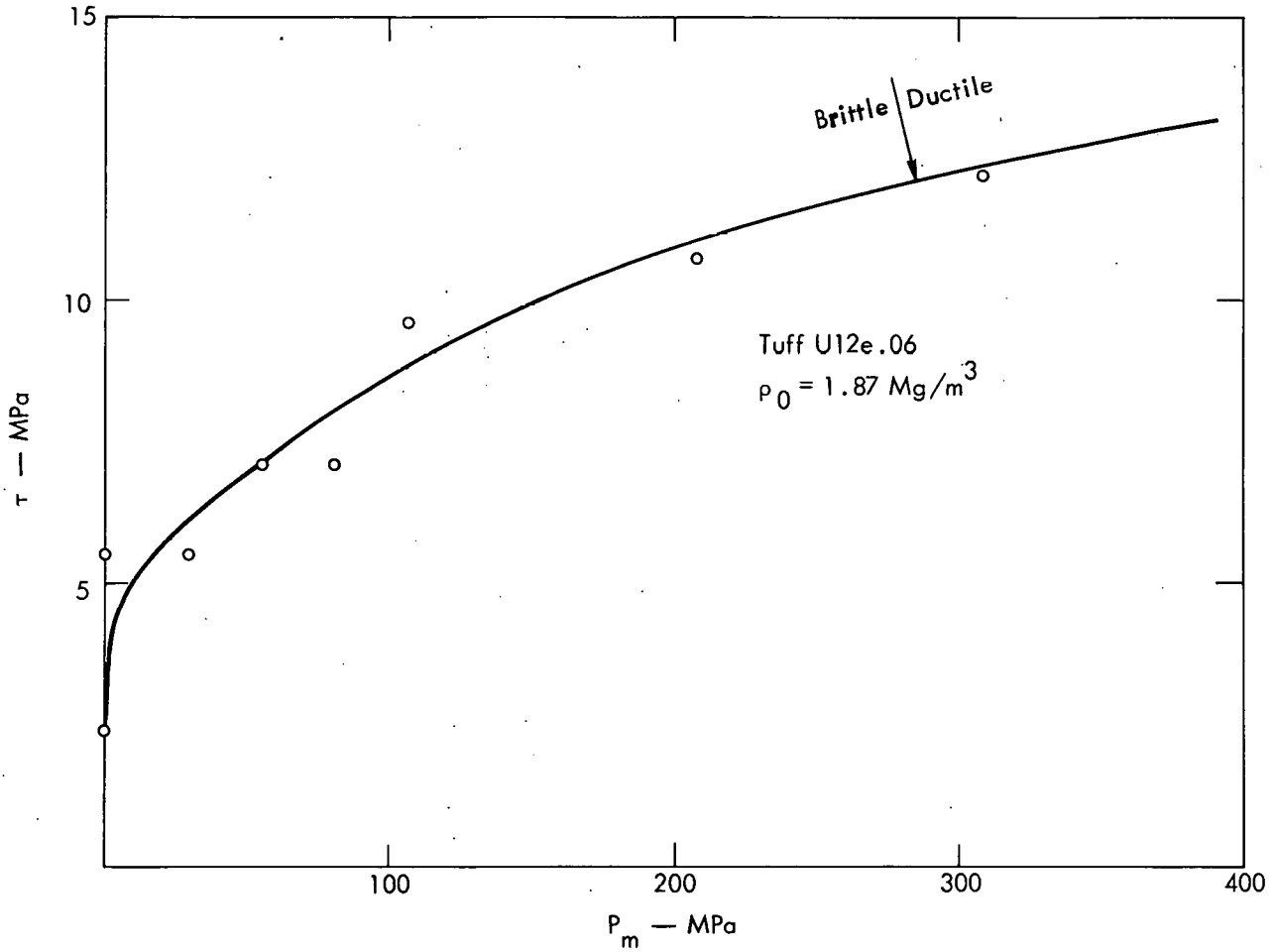

Fig. 3. Shear strength-mean pressure failure envelope for U12e.06 tuff.

Table 2. Summary of failure properties U12e.06 tuff, saturated.

Test type	σ_1 (MPa)	σ_2 (MPa)	σ_3 (MPa)	τ (MPa)	P_m (MPa)	Behavior
Brazil	3.6	0.1	-1.2	2.4	1.2	Brittle
Uniaxial compression	11	0.1	0.1	6	4	Brittle
Uniaxial compression	36	25	25	6	29	Brittle
Uniaxial compression	64	50	50	7	55	Brittle
Uniaxial compression	89	75	75	7	80	Brittle
Uniaxial compression	119	100	100	10	106	Brittle
Uniaxial compression	222	200	200	11	207	Transitional
Uniaxial compression	324	300	300	12	308	Ductile

about 20 MPa at 300 MPa mean pressure. The shear strength of the U12e.06 tuff is lower than that for saturated Mt. Helen tuff, but somewhat higher than that for the coarse-grained NTS tuffs. Stoddard (Area 2), Hudson Seal (Area 12), and Scroll (Area 19).[12] Thus, there appears to be an inverse correlation of shear strength with water content and grain size in these tuffs. The shear strength-mean pressure data for all these tuffs are compared in Fig. 4.

THREE-DIMENSIONAL STRESS-STRAIN MEASUREMENTS

The stress-strain behavior of strain-gaged samples from the core at 14.2 to 14.7 m was measured under conditions of uniaxial stress- and uniaxial strain-loading using techniques described in detail elsewhere.[3-5] Uniaxial stress loading was accomplished by axially loading the sample to failure at a constant confining pressure by the same procedure discussed in the previous section. Uniaxial strain loading is accomplished by increasing the confining pressure, while the axial stress is increased, to maintain constant radial strain. Uniaxial strain is considered to model loading by a plane shock wave; however, the strain rates under shock loading are very much larger than the ones used here. In both uniaxial stress and uniaxial strain loading, the principal strains are measured to determine loading moduli as a function of deviatoric stress and confining pressure along different loading and unloading paths.

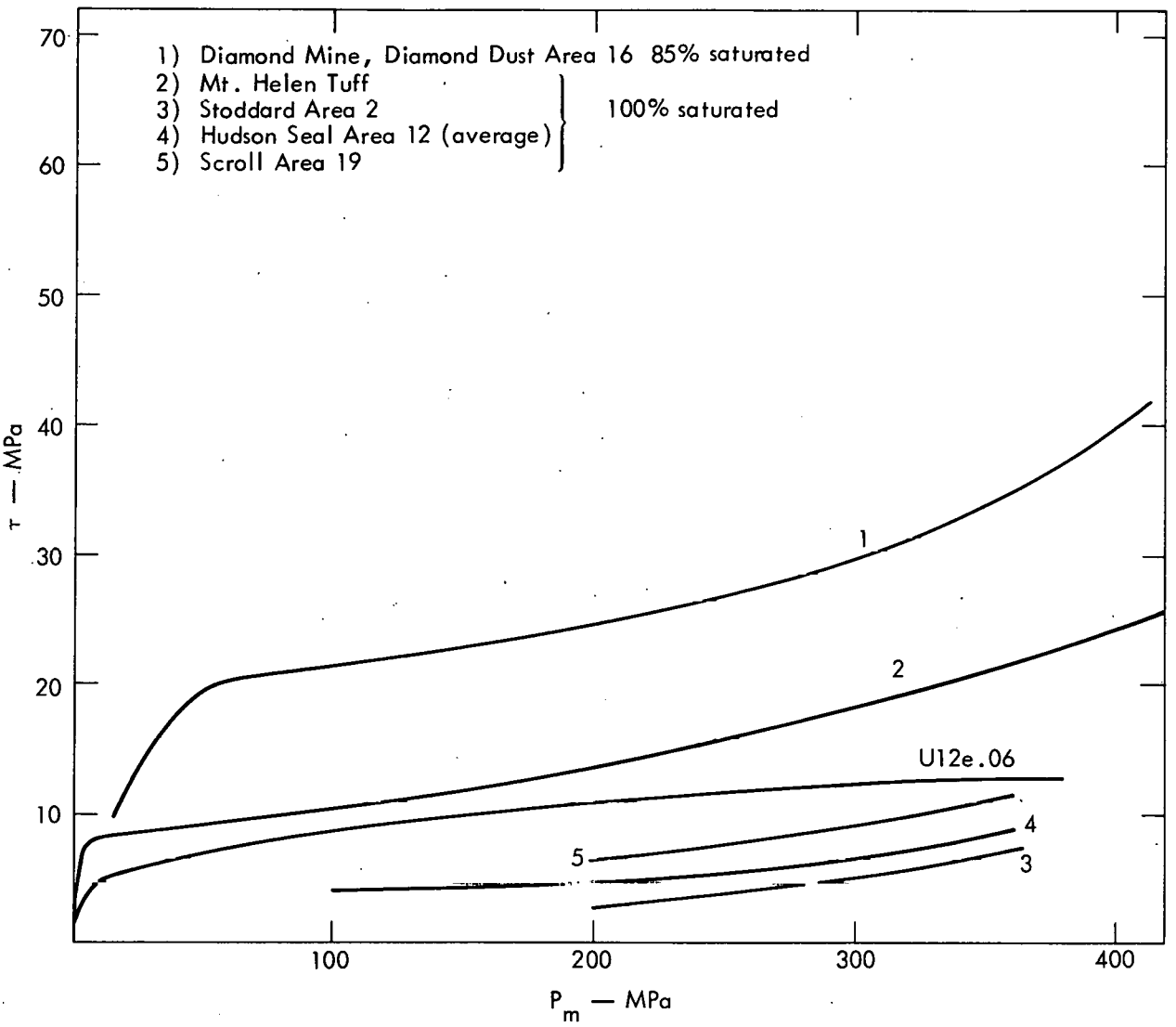

Fig. 4. Comparison of the failure envelope for U12e.06 tuff with other saturated and near-saturated tuffs.

UNIAXIAL STRESS

Tests were run at 0.1, 20, 30, 50, and 100 MPa confining pressure. Unlike the uniaxial stress measurements discussed above, the specimens were not loaded directly to failure. Rather, the samples were loaded to a stress near the failure envelope (Fig. 3), unloaded to hydrostatic conditions, and then some were recycled to either failure or near failure.

Figures 5 and 6 show the circumferential (ϵ_r) and axial (ϵ_ℓ) strain as a function of $\sigma_1 - \sigma_3$ for this tuff at confining pressures of 0.1 and 20 MPa. The test at 0.1 MPa yields an initial effective Poisson's ratio ν that is less than 0.5 (i.e., $|\epsilon_r| < 0.5\ |\epsilon_\ell|$). However, as $\sigma_1 - \sigma_3$ is increased above 1.5 MPa, ν exceeds 0.5 (i.e., $|\epsilon_r| > 0.5\ |\epsilon_\ell|$). At all higher confining pressures in this study the initial ν was greater than 0.5, an indication of dilatational behavior (Fig. 7).

Figure 7 indicates the paths followed for all 5 confining pressures in volume strain-mean pressure ($\epsilon_v - P_m$) space. The resulting behavior during initial loading is similar to that observed for the saturated Mt. Helen tuff[11] below 100 MPa; there is little or no observable compaction, and the rock apparently dilates with the first increase in axial stress. The bulk and shear moduli calculated from initial loading at each confining pressure are given in Table 3. The apparent negative bulk moduli on

Table 3. Initial loading moduli, saturated U12e.06 tuff.

	σ_3 (MPa)	μ (GPa)	K (GPa)	V_s (km/s)	V_p (km/s)
Uniaxial	0.1	0.6	4.5	0.57	1.69
Stress	20	2.7	-7.1	1.20	—
Tests	30	3.0	-3.5	1.46	—
	50	2.9	-3.4	1.45	—
	100	3.0	-1.4	1.46	—
Uniaxial strain	0.6	1.3	1.2	0.81	1.04
Tests	0.1	1.5	1.7	0.96	1.07

initial loading for the four tests above 0.1 MPa confining pressure are the consequence of the dilatational behavior on initial loading.

UNIAXIAL STRAIN

Two samples were loaded in uniaxial strain. One sample was loaded from 0.1 to 80 MPa confining pressure, then unloaded. The other was loaded from 0.6 to 420 MPa confining pressure and unloaded. Over the range of overlap the two runs are in good

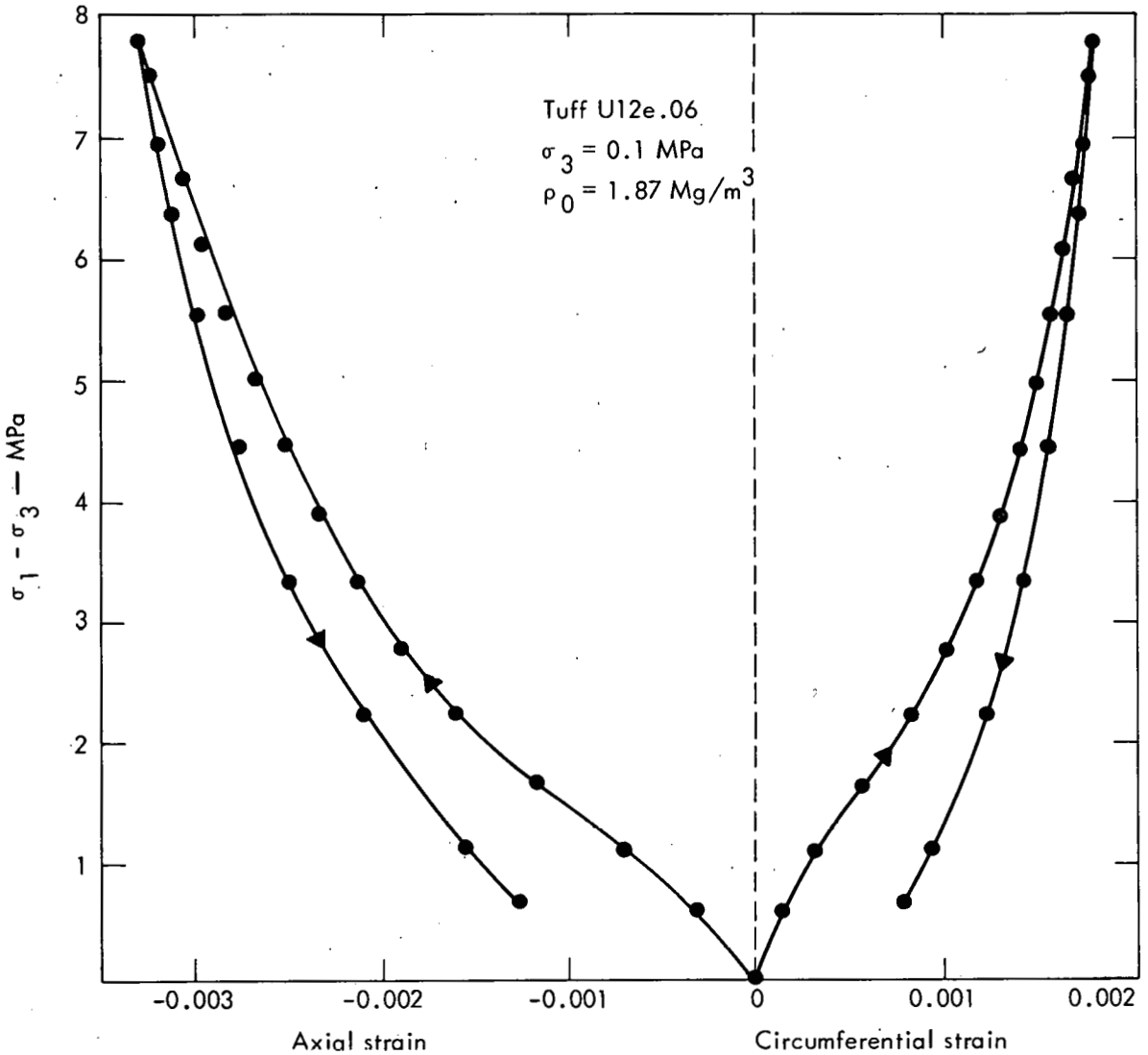

Fig. 5. Axial and circumferential strain, U12e.06 tuff, 0.1 MPa confining pressure.

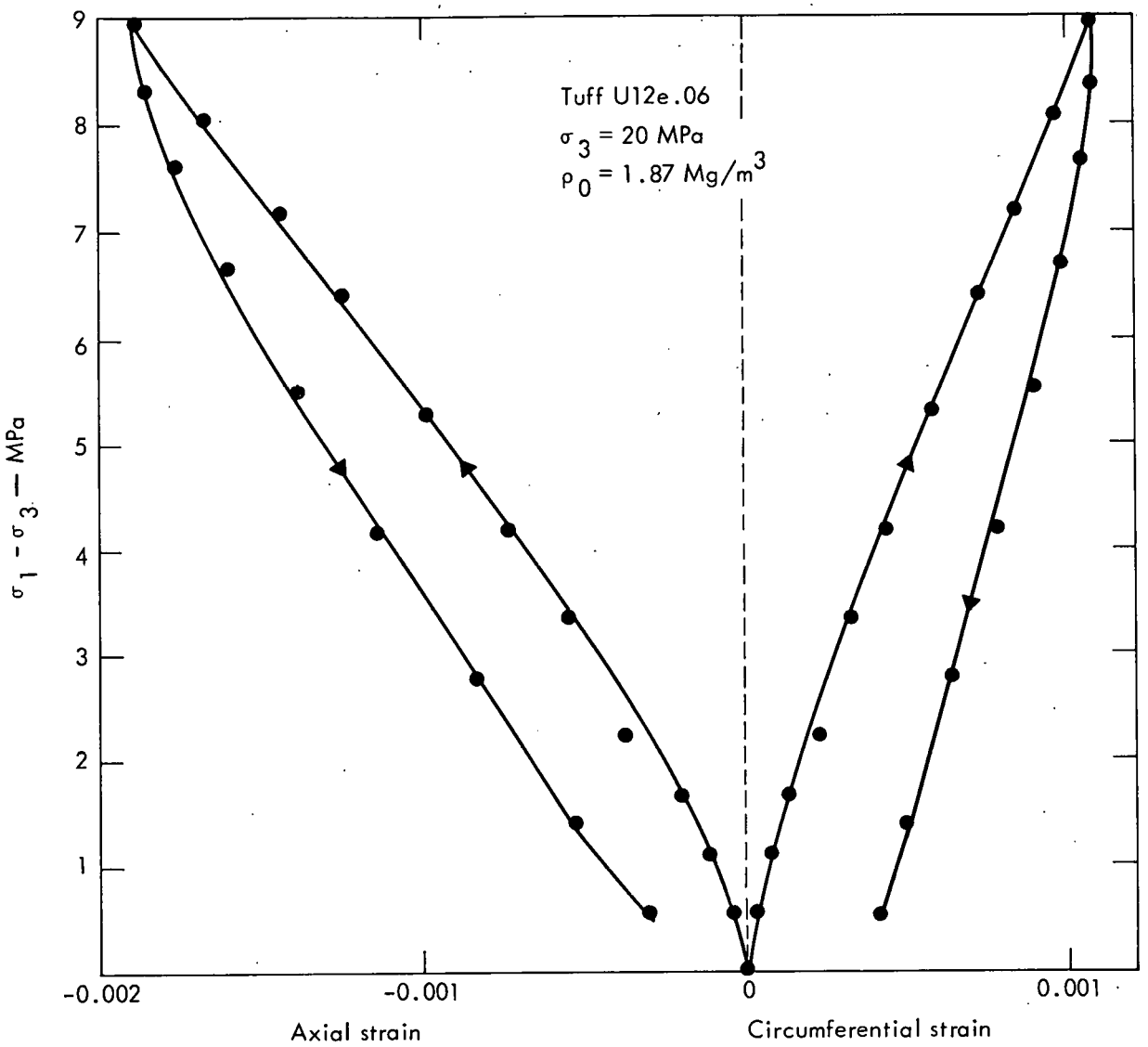

Fig. 6. Axial and circumferential strain, U12e.06 tuff, 20 MPa confining pressure.

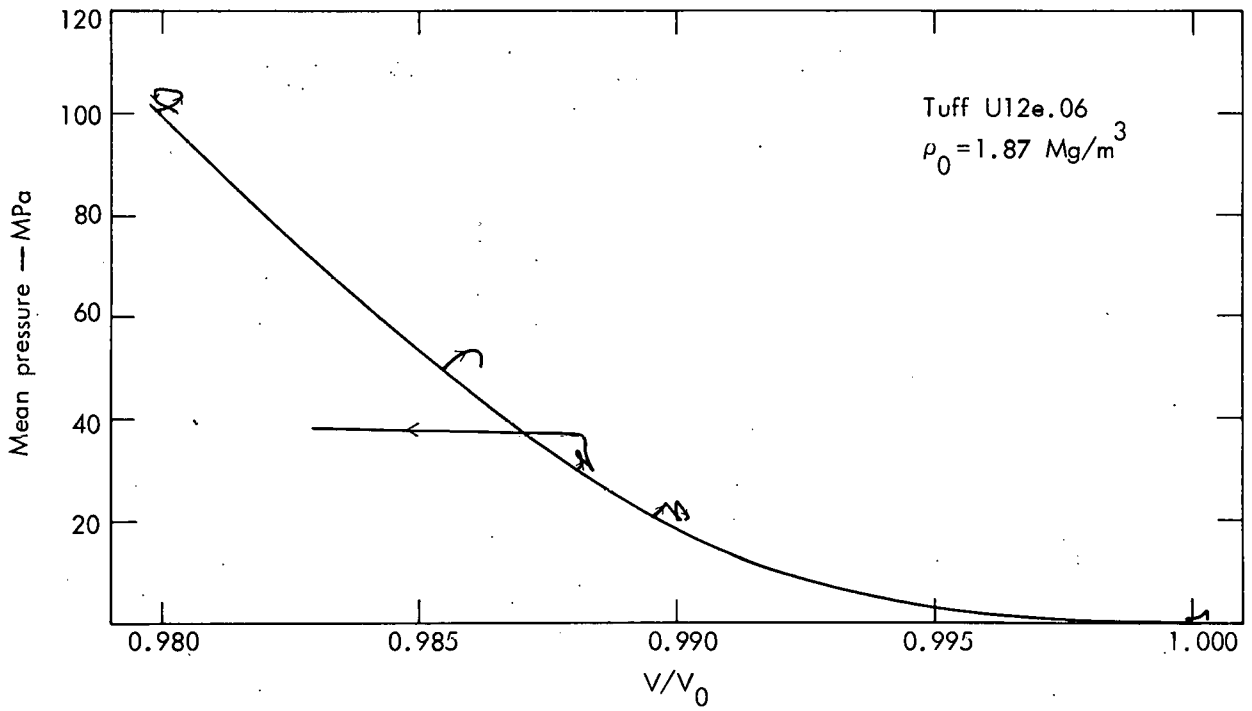

Fig. 7. Mean pressure vs volume strain for uniaxial stress tests at 0.1, 20, 30, 50, and 100 MPa. Hydrostat from Fig. 1 shown for comparison.

agreement (Figs. 8 and 10). The shear stress loading paths (Fig. 8) indicate that both samples load to stresses typical of the failure envelope and then load along that envelope to higher pressures. This phenomenon has not been observed in less porous materials such as granite and graywacke[4] but has been reported for other tuffs[10,11] and for a highly porous, dry sandstone.[13]

Since there are no shock data on the tuff from U12e.06 with which to compare, an indication of the strain rate effect on the loading behavior may be gained by comparing our uniaxial strain results with those for a nearby tuff of similar density and saturation. The tuff from a high-energy explosive site (DB7) in the Hudson Moon tunnel (U12e.12) is within 500 m of U12e.06, UG3. Both shock[14] and quasi-static[15] data exist for comparison. The wet and dry densities for this tuff (1.88 ± 0.02 and 1.53 ± 0.02 Mg/m^3, respectively)[14] compare well with those determined for the U12e.06 tuff. Figure 9 compares the hydrostats and σ_1 loading paths in uniaxial strain loading for these two tuffs. Also shown in Fig. 9 are the three points in this pressure range determined for the Hudson Moon tuff under conditions of shock loading.[14] The Hudson Moon tuff, which shows less compression under hydrostatic conditions at low pressures than the U12e.06 tuff, shows more compression with increasing pressure and has undergone 20% more compression at 300 MPa. Slightly less divergence is noted between the quasi-static σ_1 loading paths of these two tuffs in uniaxial strain. The three shock points for the Hudson Moon tuff in this pressure range indicate much less compression than the quasi-static uniaxial strain loading. Since the difference in σ_1 loading paths in uniaxial strain loading between the two tuffs is slight in comparison with the offset observed between shock and quasi-static loading, it is reasonable to assume that the shock loading data for the U12e.06 tuff would be slightly higher than that observed for the Hudson Moon tuff.

The "best fit" line[14] to the shock data is included in Fig. 9. Note that the lowest pressure point lies considerably above this line. Although data are insufficient for more than a qualitative statement, it appears that this tuff could have a "Hugoniot elastic limit" of less than 400 MPa. It should be remarked that this "best fit" line is based on data collected to 2500 MPa[14] and that some of the 18 points at higher pressure show scatter comparable to that displayed in the pressure range of Fig. 9. More low pressure data under conditions of shock loading are necessary before a definitive statement can be made.

Figure 10 compares the compression of two samples of the U12e.06 tuff in uniaxial strain under quasi-static loading with that determined from hydrostatic loading (Fig. 1). Unlike the Mt. Helen tuff[11] the axial stress curve for U12e.06 tuff loads slightly below the hydrostat at $\sigma_1 > 20$ MPa (Fig. 10). Although this is the first rock we have studied that shows this behavior, it is similar to the behavior reported by Green et al.[15] for the Hudson Moon tuff. The σ_1 loading curve is below the hydrostat, indicating that a shock loading path cannot be constructed from the hydrostat using failure data (Fig. 3). Rather, one must consider enhanced compaction in the presence of a macroscopic shear stress by using the mean pressure curve obtained under conditions of uniaxial strain. This has been demonstrated for porous sandstones that also

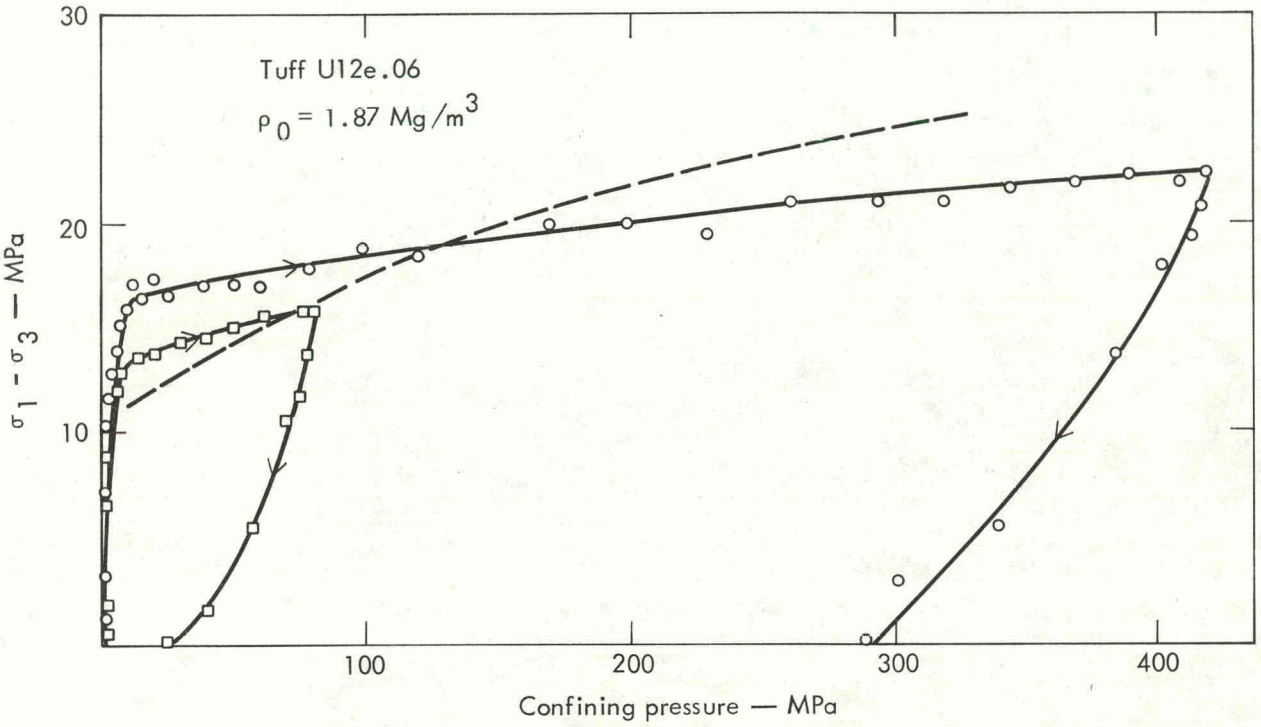

Fig. 8. Axial stress difference vs confining pressure for uniaxial strain loading tests to and from 80 and 420 MPa confining pressure. Failure envelope from Fig. 3 shown for comparison.

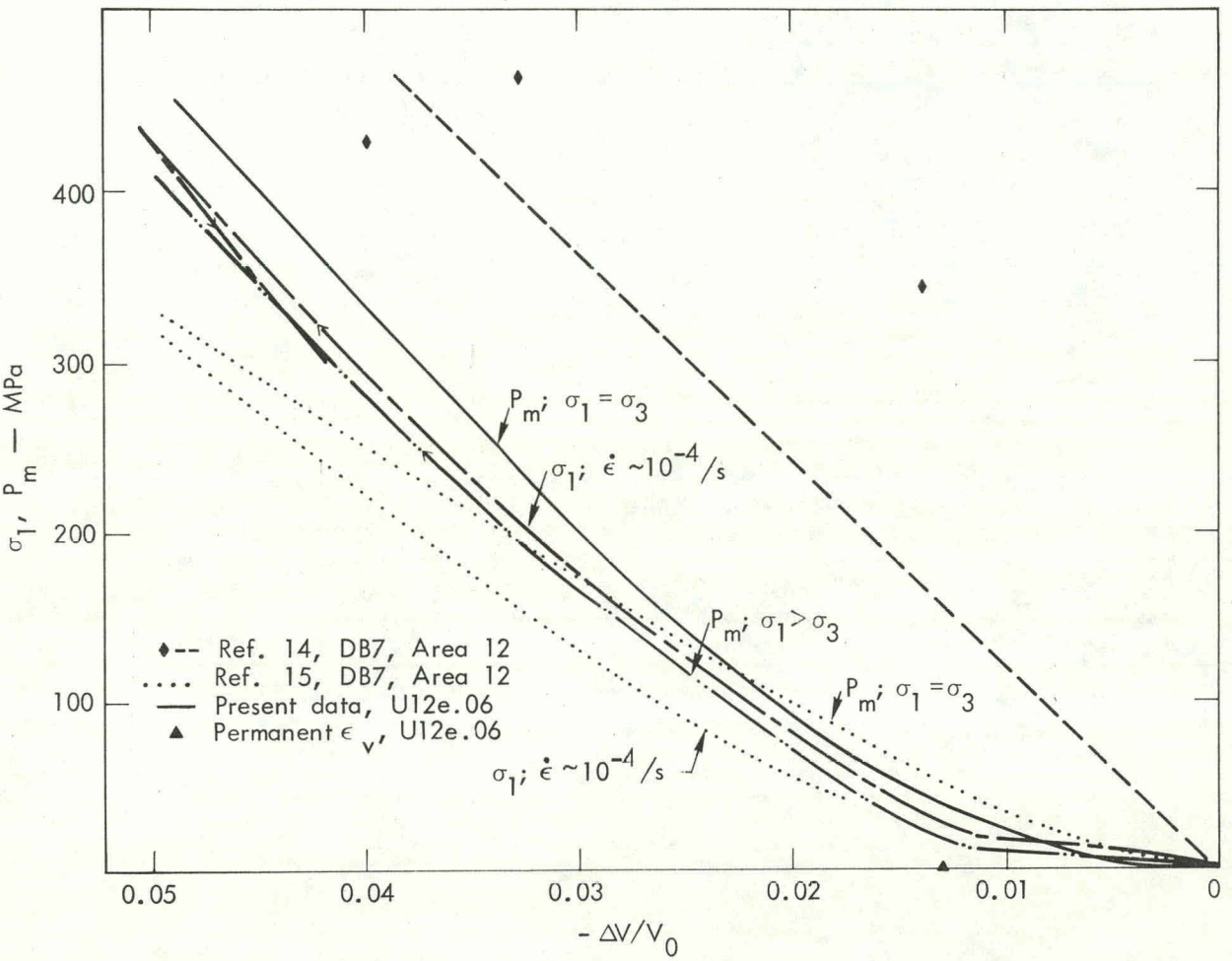

Fig. 9. Axial stress (σ_1) and mean pressure (P_m) vs volume strain for uniaxial strain loading compared with the hydrostat from Fig. 2, U12e.06 tuff. Shown for comparison are σ_1 vs volume strain for uniaxial strain loading and the hydrostat for the Hudson Moon tuff[15] as well as shock loading data for that tuff.[14]

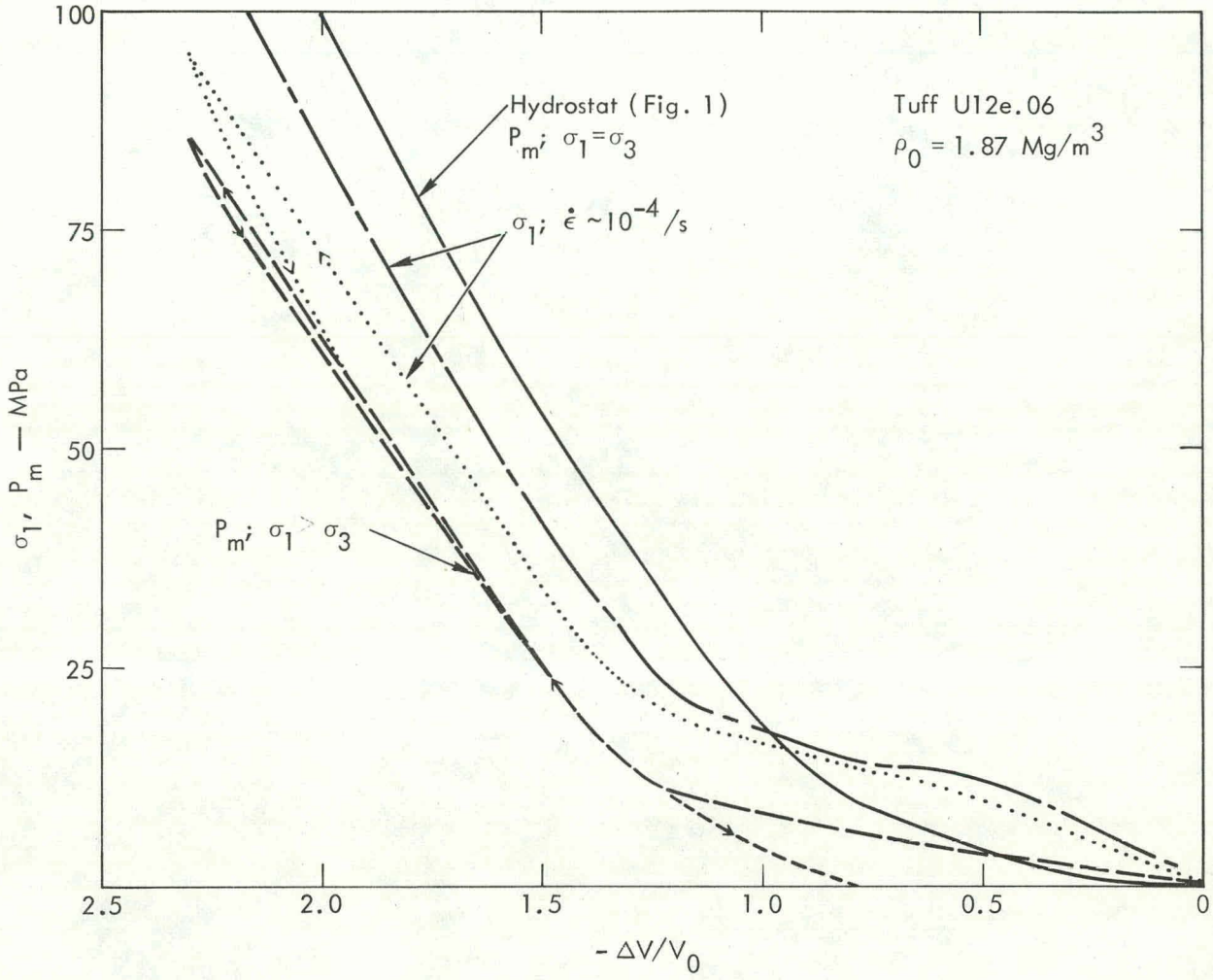

Fig. 10. Axial stress (σ_1) and mean pressure (P_m) vs volume strain for two uniaxial strain runs, U12e.06 tuff, compared with the hydrostat from Fig. 1. One P_m run omitted for clarity.

compact at high mean pressure.[4,16] However, this curve itself is likely to be strain-rate dependent and, since the failure envelope is also strain-rate dependent, calculation of a Hugoniot loading path based on low strain rate data is subject to large uncertainties.

Table 3 includes effective bulk (K) and shear (μ) moduli and the compressional (V_p) and shear (V_s) velocities calculated from stress-strain data on initial loading. The initial K from uniaxial strain loading is larger than that determined under hydrostatic loading and smaller than that determined from uniaxial stress loading. The initial μ from uniaxial strain loading is larger than that determined for uniaxial stress loading. The calculated V_p is considerably lower than the 1.92 km/s derived from seismic data[14] and is consistent with most comparisons of quasi-static laboratory and field data since Zisman's work.[17] Unfortunately, there are no laboratory ultrasonic velocity measurements on this tuff against which to compare our V_p and V_s calculated from static measurements. However, our calculated velocities are comparable to those determined from the uniaxial strain tests for the saturated Mt. Helen tuff[11] (V_p = 1.23, V_s = 0.77). The velocities determined ultrasonically at atmospheric pressure for the saturated Mt. Helen tuff were V_p = 2.60 and V_s = 1.30 and we would expect the ultrasonic velocities in the U12e.06 to be similar. The variation between velocities measured ultrasonically and those calculated from static measurements are due to cracks and pores that affect static moduli more than dynamic moduli.[18]

The permanent compactions after the uniaxial strain tests to 80 and 420 MPa were 0.8 and 1.3% respectively. The value of 1.3% compares favorably with the 1.25% observed after hydrostatic compression to 1400 MPa and indicates at least 1.3% by volume air-filled porosity in the tuff as tested. Since care was taken to maintain as-received water contents in the tuff during all stages of sample preparation and since less than 10 minutes exposure to the laboratory atmosphere was allowed for all samples, it is reasonable to assume that the tuff had at least this air-filled porosity when received.

ACKNOWLEDGMENTS

H. Louis, E. Joslyn, H. Stromberg, and H. Washington provided assistance with sample preparation and data collection. B. Bonner and R. Schock read the manuscript and provided helpful criticism. Work was performed under a contract from the Defense Nuclear Agency.

REFERENCES

1. D. R. Stephens, E. M. Lilley, and H. Louis, Int. J. Rock Mech. Min. Sci. 7, 257 (1970).
2. J. Handin and R. V. Hager, Jr., Amer. Assoc. Petrol. Geol. Bull. 41, 1 (1957).
3. A. A. Giardini, J. F. Lakner, D. R. Stephens, and H. D. Stromberg, J. Geophys. Res. 73, 1305 (1968).
4. R. N. Schock, H. C. Heard, and D. R. Stephens, Stress-Strain Behavior of a Granodiorite and Two Graywackes on Compression to 20 Kilobars, J. Geophys. Res. 78, 5922 (1973).
5. R. N. Schock and A. G. Duba, J. Appl. Phys. 43, 2204 (1972).
6. J. Handin, H. C. Heard, and J. N. Magouirk, J. Geophys. Res. 72, 611 (1967).
7. E. R. Hoskins, Int. J. Rock Mech. Min. Sci. 6, 99 (1969).
8. H. C. Heard, "The Influence of Environment on the Inelastic Behavior of Rocks," in Proc. ANS Topical Meeting, Engineering with Nuclear Explosives, Las Vegas, Nev., 1970 (American Nuclear Society, 1970), p. 127.
9. D. R. Stephens, H. C. Heard, and R. N. Schock, High-Pressure Mechanical Properties of Tuff from the Diamond Dust Site, Lawrence Livermore Laboratory, Rept. UCRL-50858 (1970).
10. H. C. Heard, R. N. Schock, and D. R. Stephens, High-Pressure Mechanical Properties of Tuff from the Diamond Mine Site, Lawrence Livermore Laboratory, Rept. UCRL-51099 (1971).
11. H. C. Heard, B. P. Bonner, A. Duba, R. N. Schock, and D. R. Stephens, High-Pressure Mechanical Properties of Mt. Helen Tuff, Nevada, Lawrence Livermore Laboratory, Rept. UCID-16261 (1973).
12. H. C. Heard, H. D. Stromberg, and H. R. Washington, Strength of Stoddard, Hudson Seal and Scroll Tuffs, University of Calif., PMD Note 323 (1968).
13. A. Duba, A. E. Abey, B. P. Bonner, H. C. Heard, and R. N. Schock, High Pressure Mechanical Properties of Kayenta Sandstone, Mesa County, Colorado, Lawrence Livermore Laboratory, Rept. in preparation.
14. N. H. Froula, E. L. Suenaga, and R. L. Bryson, Shock Compression and Release Behavior of Two Nevada Test Site Tuffs, Systems, Science and Software, La Jolla, Calif., Rept. DNA 2851F (1972).
15. S. J. Green, R. M. Griffin, A. D. Black, S. W. Butters, S. W. Duncan, H. R. Pratt, and K. B. Watson, High-Pressure Properties of Several Nevada Test Site Tuffs, Terra Tek, Inc., Salt Lake City, Utah, Rept. DNA 2814F (1971).
16. R. N. Schock, H. C. Heard, and D. R. Stephens, Mechanical Properties of Rocks from the Rio Blanco Stimulation Experiment, Lawrence Livermore Laboratory, Rept. UCRL-51260 (1972).
17. W. A. Zisman, Proc. Natl. Acad. Sci. 19, 680 (1933).
18. G. Simmons and W. F. Brace, J. Geophys. Res. 70, 5649 (1965).

DISTRIBUTION

LLL Internal Distribution

Roger E. Batzel, L-1
J. Kane/G. Dorough, L-401
A. Abey, L-437 (15)
B. Bonner, L-437
J. Bryan, L-51
T. Butkovich, L-43
J. Carothers, L-7
R. Chin, L-51
B. Crowley, L-42
M. Cunningham, L-40
A. Duba, L-437 (20)
D. Emerson, L-47
L. Germain, L-18
C. Groseclose/H. Reynolds, L-21
J. Hannon, L-41
B. Hudson, L-40
H. Heard, L-437 (15)
J. Hearst, L-41
R. Heckman L-437 (2)
A. Holzer, L-41
J. Kahn, L-41
E. Joslyn, L-437
D. Larson, L-41
A. Lewis, L-43
E. Lilley, L-437
A. Maimoni, L-503
R. McArthur, L-777
W. McMaster, L-40
D. Norris, L-90
A. Piwinskii, L-437
L. Ramspott, L-44
A. Ratcliffe, L-40
H. Rodean, L-41
J. Schatz, L-44
R. Schock, L-437 (10)
D. Springer, L-41
D. Stephens, L-437
H. Stromberg, L-424
R. Terhune, L-47
M. Van Thiel, L-504
H. Washington, L-437
G. Werth, L-13
L. Wight, L-90
M. Zaslawsky, L-424
TID File, L-3 (30)

External Distribution

J. Zelasko
J. Ehrgott
U.S. Army Engineer Waterways
Experiment Station
Corps of Engineers
Vicksburg, Mississippi 39180

E. Willis
C. Romney
J. T. Jones
Advanced Research Projects Agency
Arlington, Virginia 22209

T. Stong
D. Oakley
C. McFarland
J. Lewis
Defense Nuclear Agency
Washington, D.C. 20305

B. Brown
W. Davis
B. Grote
Defense Nuclear Agency
Albuquerque, New Mexico 87115

R. A. Black
S. Ruby
D. C. Russell
J. Pearce
Advanced Research Projects Agency
Washington, D.C. 20301

J. Trulio
Applied Theory, Inc.
Los Angeles, California 90024

R. McQueen
Los Alamos Scientific Laboratory
Los Alamos, New Mexico 87544

C. Godfrey
R. Swift
Physics International Company
San Leandro, California 94577

H. L. Brode
The Rand Corporation
Santa Monica, California 90401

E. A. Martinelli
J. E. Whitener
H. Cooper
R and D Associates
Santa Monica, California 90403

P. Hoekstra
E. Chamberlain
U.S. Army Terrestrial Sciences Center
Hanover, New Hampshire 03755

D. Baron
I. Nelson
Paul Weidlinger Consulting Engineer
New York, N.Y. 10022

J. Isenberg
Agbabian-Jacobsen Associates
Los Angeles, California 90045

R. E. Duff
D. Rinney
Systems, Science and Software
La Jolla, California 92037

S. Green
Terra Tek
Salt Lake City, Utah 84410

C. F. Peterson
Stanford Research Institute
Menlo Park, California 92605

R. H. Gates
U.S. Army Engineers
Livermore, California 94550

T. A. Weaver
Los Alamos Scientific Laboratory
Los Alamos, New Mexico 97544

J. Lacombe
Defense Nuclear Agency
Mercury, Nevada 89104

D. L. Hoover
U.S. Geological Survey
Mercury, Nevada 89104

P. Dai
TRW Systems Group
600 East Mill Street
San Bernardino, California 92409

Technical Information Center (2)
Oak Ridge, Tennessee

BWH/rt